

The in vitro and in vivo performance of a strontium-containing coating on the low-modulus Ti35Nb2Ta3Zr alloy formed by micro-arc oxidation

Wei Liu¹ · Mengqi Cheng¹ · Tuerhongjiang Wahafu¹ · Yaochao Zhao¹ · Hui Qin¹ · Jiaying Wang¹ · Xianlong Zhang¹ · Liqiang Wang²

Received: 26 March 2015 / Accepted: 27 June 2015 / Published online: 8 July 2015
© Springer Science+Business Media New York 2015

Abstract The β -titanium alloy is thought to be a promising alloy using as orthopedic or dental implants owing to its characteristics, which contains low elastic modulus, high corrosion resistance and well biocompatibility. Our previous study has reported that a new β -titanium alloy Ti35Nb2Ta3Zr showed low modulus close to human bone, equal tissue compatibility to a traditional implant alloy Ti6Al4V. In this study, micro-arc oxidation (MAO) was applied on the Ti35Nb2Ta3Zr alloy to enhance its surface characteristics and biocompatibility and osseointegration ability. Two different coatings were formed, TiO₂ doped with calcium–phosphate coating (Ca–P) and calcium–phosphate–strontium coating (Ca–P–Sr). Then we evaluated the effects of the MAO coatings on the Ti35Nb2Ta3Zr alloy through in vitro and in vivo tests. As to the characteristics of the coatings, the morphology, chemical composition, surface roughness and contact angle of MAO coatings were tested by scanning electron microscopy, energy dispersive spectroscopy, atomic force microscopy, and video contact-angle measurement system respectively. Besides, we performed MTT assay, ALP test and cell morphology-adhesion test on materials to evaluate

the MAOed coating materials' biocompatibility in vitro. The in vivo experiment was performed through rabbit model. Alloys were implanted into rabbits' femur shafts, then we performed micro-CT, histological and sequential fluorescent labeling analysis to evaluate implants' osseointegration ability in vivo. Finally, the Ca–P specimens and Ca–P–Sr specimens exhibited a significant enhancement in surface roughness, hydrophilicity, cell proliferation, cell adhesion. More new bone was found around the Ca–P–Sr coated alloy than Ca–P coated alloy and Ti35Nb2Ta3Zr alloy. In conclusion, the MAO treatment improved in vitro and in vivo performance of Ti35Nb2Ta3Zr alloy. The Ca–P–Sr coating may be a promising modified surface formed by MAO for the novel β -titanium alloy Ti35Nb2Ta3Zr.

1 Introduction

Traditional titanium and its alloys have been widely applied in orthopedic or dental from last century because of their chemical stability and good biocompatibility [1, 2]. Despite the success in the use of traditional titanium and its alloys, some drawbacks still exist, among which the high elastic modulus (110 Gpa) of the Ti6Al4V (a widely used $\alpha + \beta$ type titanium alloy) was thought to be a main one [3]. Relative high elastic modulus may result in stress shielding when unbalance force distributes between bone and implants [4]. Besides, vanadium and aluminum elements which Ti6Al4V contains have been reported toxic to human body [5, 6].

In recent years, β -titanium was thought to be a better choice for medical appliance for its low elastic modulus and non-toxic element compared with Ti6Al4V [7]. A

Wei Liu and Mengqi Cheng have contributed equally to this work.

✉ Xianlong Zhang
zhangxianlong2013s@163.com

✉ Liqiang Wang
liqiangwang8000@126.com

¹ Department of Orthopedic, Shanghai Jiao Tong University Affiliated Sixth People's Hospital, 600 Yishan Road, Shanghai 200233, People's Republic of China

² State Key Laboratory of Metal Matrix Composites, Shanghai Jiao Tong University, 800 Dongchuan Road, Shanghai 200244, People's Republic of China

novel β -titanium Ti35Nb2Ta3Zr we reported previously showed a low elastic modulus (48 GPa) [8] close to human bone (10–30 GPa) and equally tissue compatibility compared to Ti6Al4V [3]. Though the mechanical properties of Ti35Nb2Ta3Zr alloy were better than Ti6Al4V, the biological performance especially the ability of bone integration was in a relative low level [9].

The surface modified technology was a good way to improve alloys' surface morphology, chemical composition and microstructure, which were thought to be important factors for implants' biological performance [10, 11]. Calcium–phosphate ceramic are usually coated on the titanium alloys for its bioactivity on bone formation and bonding [12]. Several methods have been applied in synthesizing coatings on alloys' surface, including plasma spraying, ion implanting, alkali heating, hydrothermal treatment, micro-arc oxidation (MAO) and so on [13–15]. The MAO is an electrochemical method that can not only synthesize a porous, rough, hydrophilic coating on material's surface [16], but also incorporate some elements such as silver, zinc or strontium (Sr) into coatings [17–19].

It was reported that strontium can improve biological performance of titanium alloys. Strontium is somehow like calcium, it is a trace metal which is stored in bone in human body [20]. The strontium salts are widely used as a treatment for the postmenopausal osteoporosis [21]. Some studies argued that strontium can stimulate bone formation and inhibit bone resorption [22, 23]. Moreover, various strontium-containing materials were synthesized to evaluate its bone forming ability, which turned out that strontium seemed to enhance bone formation [24–28].

In the present study, the MAO was performed for the new β -titanium Ti35Nb2Ta3Zr to synthesize TiO₂ layer doped with calcium–phosphate (Ca–P) or calcium–phosphate–strontium (Ca–P–Sr) on the surface of alloys. Then the in vitro and in vivo tests were performed to determine the biological performance of the MAOed Ca–P and Ca–P–Sr Ti35Nb2Ta3Zr alloy through cell tests and animal experiments.

2 Materials and methods

2.1 Materials

The Ti35Nb2Ta3Zr alloy was synthesized when high purity sponge of Ti (99.95 %, Bao Ti Group, China), a billet of Ti–Nb inter-alloy (Bao Ti Group, China), high purity billets of Ta (99.8 %, Bao Ti Group, China) and Zr (99.9 %, Bao Ti Group, China) were mixed and melt in a vacuum consumable arc melting furnace for three times for 60 min at 1223 K to homogenize the chemical composition

in an vacuum condition. The specimens were polished with a series of increasingly finer emery papers up to 1200 grit. Then we cleaned specimens ultrasonically in acetone, ethanol and de-ionized water. Alloys were sterilized before experiment.

2.2 Preparation of micro-arc oxidation coatings

Prior to the MAO process, the TNTZ alloys were ground with sandpapers, ultrasonically washed with acetone and de-ionized water, then hot-air dried. The MAO process to synthesize Ca–P–Sr TNTZ alloys was performed when TNTZ alloys were subjected in an aqueous electrolyte containing NaH₂PO₄ 0.04 mol/L; Ca(CH₃COO)₂ 0.1 mol/L; Sr(CH₃COO)₂ 0.04 mol/L. For the Ca–P–Sr coated group, the pulse voltage, frequency, and oxidizing time were set as 420 V, 200 Hz, and 5 min. As to the Ca–P coated group, no Sr(CH₃COO)₂ in the aqueous electrolyte, the samples were prepared at 360 V for 5 min and the pulse frequency was fixed at 200 Hz. After the MAO treatment, all the alloys were washed with distilled water and dried. Then we cut the alloys into plates (diameter: 13 mm; thickness: 1 mm) and rods (diameter: 3 mm; length: 8 mm) for in vitro and in vivo studies, respectively. All samples were sterilized before in vitro and in vivo experiment.

2.3 Characterization of MAOed coatings

The surface morphology was imaged using a field-emission scanning electron microscope (FESEM, FEI NOVA NanoSEM) at 5 kV. The energy dispersive spectroscope (EDS, INCA Energy, Oxford Instruments, Oxford, Britain) was done to analyze the chemical composition of the coatings. The surface roughness (Ra) and contact angle were determined (three specimens for each type of materials, five random places one specimen) using atomic force microscopy (AFM, Nano scope 3; Bruker, Germany) and a video contact-angle measurement system respectively.

2.4 Cell culture

The MG63 cells (Cell Bank of Type Culture Collection of Chinese Academy of Sciences) were cultured in Dulbecco's modified Eagle's medium (DMEM) with 10 % FBS (fetal bovine serum, Gibco) and 1 % penicillin/streptomycin in a humidified atmosphere of 5 % CO₂ at 37 °C. The culture medium was replaced at regular intervals (2–3 days). Regarding cell differentiation test, the osteogenic media (regular media supplemented with 10 mM β -glycerol phosphate, 0.2 mM ascorbic acid, and 10⁻⁸ M dexamethasone (Sigma)) was applied.

2.5 MTT assay

The quantitative colorimetric test-methylthiazol tetrazolium (MTT) test was performed to evaluate cell viability. Cells were seeded on the specimens (five specimens for each alloy at each time point) at 2×10^4 cells per ml and cultured for 1, 4, 8 and 16 days. When the incubation time was over, we removed the culture medium, rinsed the samples three times with PBS. Then 10 μ l MTT solution was added to the culture at the prescribed time for 4 h to form formazan. Then the medium was aspirated and dimethyl sulfoxide (DMSO) was used to dissolve the dark blue crystals. The optical density (OD) was measured at wavelength of 570 nm using an ELISA reader.

2.6 ALP activity

The differentiation behavior of MG63 cells was estimated by measuring ALP activity. Cells were seeded on specimens at 2×10^4 cells per ml in a 24-well plate. The ALP test was performed after the cells were cultured for 4, 8 and 16 days by measuring the transformation of *p*-nitrophenyl-phosphate (pNPP) into *p*-nitrophenol (pNP). Following the prescribed incubation time, cells were rinsed 3 times with PBS and lysed in 0.1 % Triton X-100 (Sigma) by using standard freeze–thaw cycling. Fifty microliters of the sample were mixed with 50 μ l of freshly prepared pNPP substrate (1 mg/ml) and incubated at 37 °C for 30 min. The reaction was stopped by the addition of 50 μ l of 0.2 M NaOH. The amount of pNP produced was quantified by measuring the absorbance at 405 nm in an ELISA reader. The BCA protein assay kit was used to measure the total protein content. The ALP activity was normalized to the total protein amounts at each selected incubation time.

2.7 Cell morphology on materials

After the MG63 cells were seeded on the alloy sample discs at 1×10^4 cells cm^{-2} and cultured for 12 h. Then cells on the materials were fixed with 2.5 % glutaraldehyde in 0.1 M PBS buffer (pH 7.4) for 20 min, and washed three times with PBS for 5 min at room temperature. Afterward, each sample was dehydrated by graded dehydration and absolutely pure ethyl alcohol for 10 min at room temperature, and then the samples were dried with CO_2 and sputter-coated with a gold–palladium layer for SEM analysis (FESEM, FEI NOVA NanoSEM). The scanning electron microscopy (SEM) examinations of cells cultured on the surface of specimens were performed to show the cells' morphology, adhesion and spreading ability. Cell numbers were counted in five random fields on each sample.

2.8 Animal experiments

Twelve adult New Zealand White rabbits were used in this study. All the animal experiments were approved by the Animal Care Committee of Shanghai Jiao Tong University Affiliated Sixth People's Hospital and performed according to the animal welfare legislation of the People's Republic of China. The animals were anesthetized with pentobarbital (25 mg/kg) by intravenous injection. Femur shafts were used as implantation sites. The surgical site was shaved and disinfected using Iodine prior to the incision. Incision was begun in the lateral femur shaft, then we prepared an implantation site at 3–4 cm distal to the proximal or distal femur diaphysis using the drill. Then implants were pressed fit to the holes (two implants per femur). After the implantation process, the incision was closed. All the processes were completed using aseptic technique. Cefazolin sodium (20 mg/kg) was injected to the animal by intramuscular way when the surgery was over. The Alizarin Red S (30 mg/kg) (Sigma) and Calcein (20 mg/kg) (Sigma) were intraperitoneally injected to the rabbits 3 and 9 weeks post-operation, respectively, to label the newly forming bone. Animals were sacrificed through the intravenous injection of an overdose pentobarbital sodium at 12 weeks post operation.

2.8.1 Micro-CT evaluation

When experimental rabbits were killed, femurs contained implants were harvested. Then micro-computerized tomography (micro-CT) was employed to evaluate newly forming bone around the implants by a Sky Scan 1172 high-resolution micro-CT scanner (Sky Scan NV), equipped with a 100 kV/100 μ A X-ray source at an isotropic voxel size of 18 μ m. We acquired the data of the two-dimensional (2D) images directly from the scans, and then the three-dimensional (3D) images were reconstructed around the volume of interest (VOI) which was set as a ring from the implant surface with radius of 1 mm using CTVol software (Sky scan Company). The multilevel threshold procedures were applied to distinguish bones from other tissues. Bone volume/total volume (BV/TV), trabecular thickness (Tb.Th) and trabecular number (Tb.N) were assessed.

2.8.2 Histological evaluation and fluorescent labeling analysis

After experimental rabbits were sacrificed, femurs were harvested and fixed in 10 % buffered formalin. Then tissues were dehydrated stepwise for in 70, 95, or 100 % ethanol, followed by incubation in methyl methacrylate

resin. A Leica diamond saw (Leica SP1600) was used to cut the resin blocks into 150 μm , perpendicular to the long axis of the femoral shaft. Then we grounded and polished the sections to a thickness about 50 μm . The fluorescence markers were evaluated using a confocal laser scanning microscopy (Leica CLSM). 543/617, 488/517 nm were employed as the excitation/emission wavelengths of chelating fluorochromes for Alizarin Red S and Calcein respectively. Finally, we stained the specimens with toluidine blue. The final slices were observed using a Leica microscope (Leica DM400).

2.9 Statistical analysis

Statistical analysis processes were conducted with SPSS 20.0. The count data was presented as mean \pm standard deviation. Differences between groups were analyzed using one-way ANOVA followed by SNK test. $P < 0.05$ was considered to indicate statistically significant differences.

3 Results

3.1 Surface characterization and morphology

The surface morphology of the Ca–P Ti35Nb2Ta3Zr (Ca–P), Ca–P–Sr Ti35Nb2Ta3Zr (Ca–P–Sr) and Ti35Nb2Ta3Zr (TNTZ) alloy were observed by the electron scanning microscopy (SEM). Compared to TNTZ alloy, the MAOed alloy Ca–P and Ca–P–Sr exhibited a porous surface (Fig. 1). The chemical compositions of the two MAOed specimens' surfaces were determined by the energy dispersive spectroscope (EDS). The results showed that Ca and P were added to the MAOed specimens' surface. Besides, the strontium element was also detected in the Ca–P–Sr specimens with a weight up to 8 wt%. More details on Fig. 2. The surface roughness (Ra) was measured by AFM, which turned out that the MAO process enhanced the surface roughness comparing with the TNTZ alloy (Fig. 3a). Ra values of the alloys were 45.52 ± 9.09 nm, 199.44 ± 14.38 nm, 193.38 ± 13.37 nm for TNTZ, Ca–P and Ca–P–Sr groups respectively. Wettability of the MAO specimens was also studied. The data showed that the MAO process decreased the water contact angles (Fig. 3b). The contact angles were $39.2^\circ \pm 2.9^\circ$, $28.7^\circ \pm 2.9^\circ$, $27.8^\circ \pm 3.9^\circ$ for TNTZ, Ca–P and Ca–P–Sr groups respectively.

3.2 In vitro biocompatibility

The in vitro biocompatibility of the materials was determined through the MTT, ALP and cell adhesion tests. The outcomes of the in vitro tests proved that the MAO

procedure increased the biocompatibility of the materials in vitro.

3.2.1 MTT results

The cell viability was reflected by MTT test, which was performed at the day 1, 4, 8 and 16. There was no significant difference was found among the three specimens at day 1 and 4 (Fig. 3c). Then significant difference was detected at day 8 and 16 between the TNTZ and MAOed specimens. Compared with other groups, the Ca–P–Sr group showed the highest cell viability (Fig. 3c).

3.2.2 ALP activity

The alkaline phosphatase activity, which was thought to be a reflection of the osteoblast differentiation, was measured at day 4, 8 and 16. At day 4, the ALP activity of Ca–P–Sr group (not Ca–P group) was higher than the TNTZ group. Then MAO coated specimens showed higher ALP activity than TNTZ alloy at day 8 and 16. Similar to the MTT test, the Ca–P–Sr group had the highest ALP activity through the test (Fig. 3d).

3.2.3 The morphology of cells attached on materials

The SEM was used to observe the morphology of cells attached on materials after 12 h culture. We can acquire the details from figure that cells spread more diversely and flatter in Ca–P and Ca–P–Sr groups than the TNTZ alloy (Fig. 4). Contrast to TNTZ alloy, Ca–P and Ca–P–Sr groups exhibited not only more cells on the surface but also cells with longer and thinner pseudopodia (no difference between Ca–P and Ca–P–Sr groups) (Fig. 4), which indicated that the Ca–P and Ca–P–Sr groups showed a better ability for cell adhesion and spread than TNTZ alloy.

3.3 In vivo biocompatibility

3.3.1 Micro-CT analysis

The implants' position and new bone formation around the implants were evaluated by X-ray and micro-CT. All the implants were in position (Fig. 7a). As the 2D images and high resolution 3D reconstruction images showed more new bone around the implants in MAOed groups than TNTZ alloy (Fig. 5). The Ca–P–Sr group presented the highest new BV. To be specific, the BV/TV ratio of Ca–P–Sr group reached 31.7 ± 5.2 %, which was significant higher than Ca–P group (24.4 ± 4.2 %) and TNTZ group (17.5 ± 3.0 %) (Fig. 6a). Similar to BV/TV, the values of Tb.Th and Tb.N were significant higher in Ca–P–Sr group (148.6 ± 17.8 μm , 2.6 ± 0.3 mm^{-1} , respectively) than

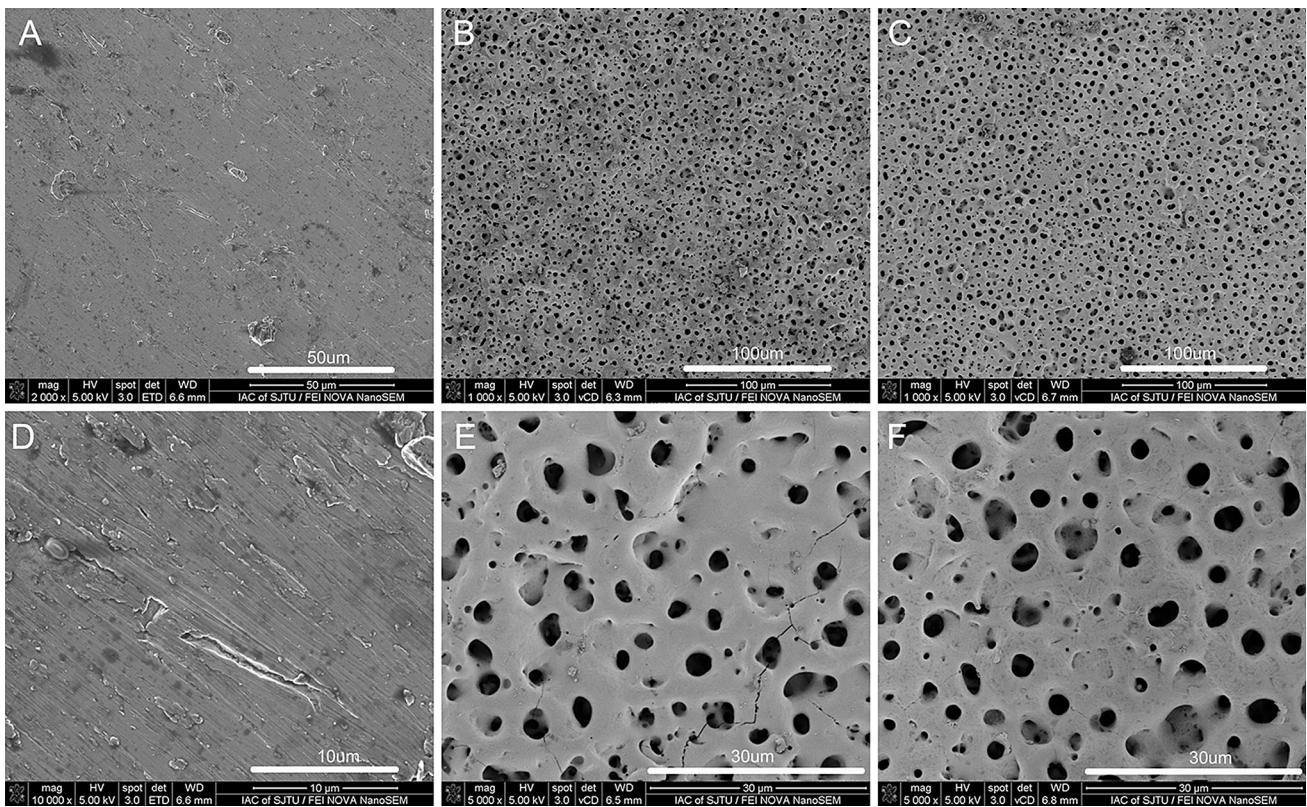


Fig. 1 SEM images of surface morphology of TNTZ group (a, d), Ca-P group (b, e), Ca-P-Sr group (c, f). Abbreviations: SEM scanning electron microscope, TNTZ Ti35Nb2Ta3Zr alloy

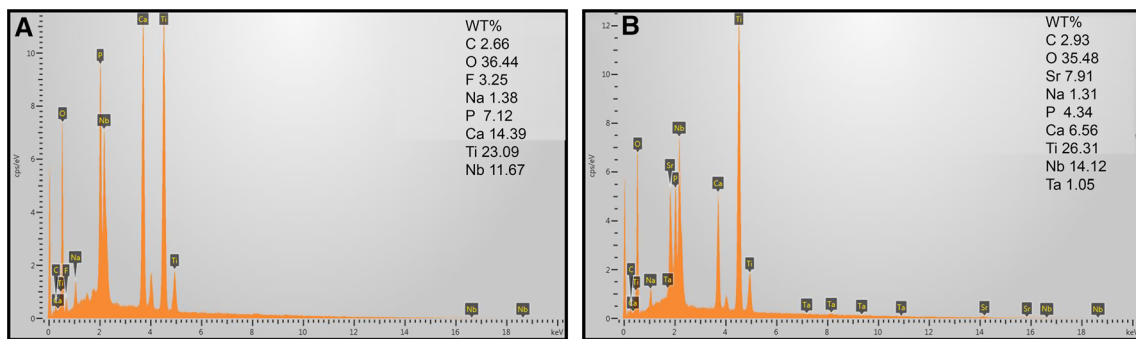


Fig. 2 EDS results of the Ca-P group (a) and Ca-P-Sr group (b). Abbreviations: EDS energy dispersive spectroscopy

Ca-P group ($116.3 \pm 13.0 \mu\text{m}$, $1.9 \pm 0.3 \text{ mm}^{-1}$, respectively) and TNTZ group ($77.3 \pm 6.7 \mu\text{m}$, $0.8 \pm 0.2 \text{ mm}^{-1}$ respectively). More details on Fig. 6.

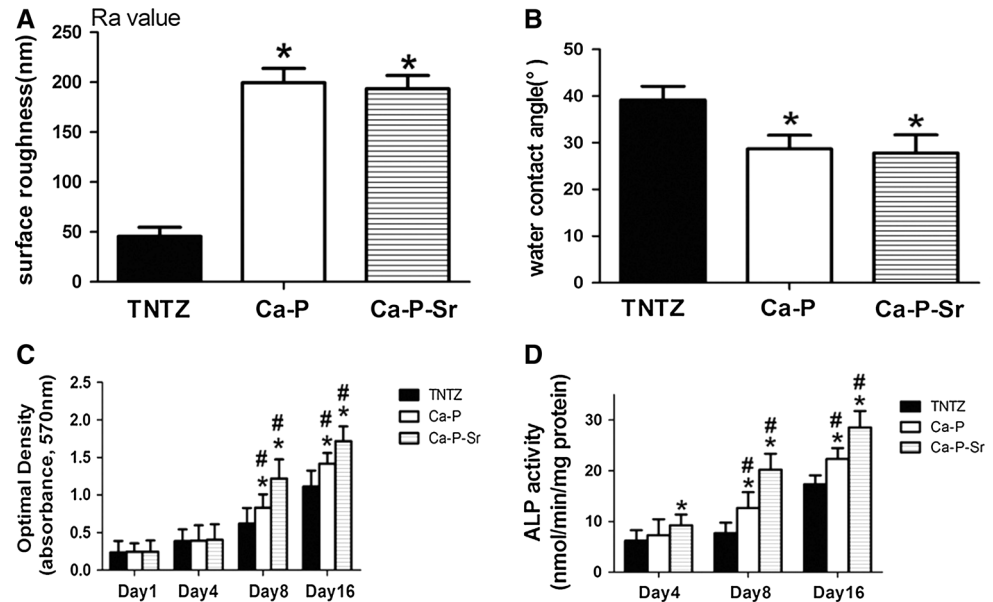
3.3.2 Histology evaluation and Fluorescent labeling analysis

Histological analysis was done to evaluate new bone formation around the implants through toluidine blue staining. Figure 7b exhibited that new bone formed directly around the implant. Compared to Ca-P-Sr and Ca-P groups,

obvious space was observed between newly forming bone and implant in the TNTZ group (Fig. 8). Besides, the new bone area and bone-implant contact were calculated through the figures. Consistent with the micro-CT results, the Ca-P-Sr group ($37.8 \pm 6.2 \%$) presented higher new bone area than Ca-P ($28.1 \pm 4.8 \%$) and TNTZ ($18.9 \pm 4.5 \%$) groups (Fig. 7c), bone-implant contact also exhibited a higher rate in Ca-P-Sr group ($37.3 \pm 5.0 \%$) than Ca-P ($24.7 \pm 4.7 \%$) and TNTZ ($19.2 \pm 3.3 \%$) groups (Fig. 7d).

As to sequential fluorescent labeling analysis, the confocal laser scanning microscopy was employed. Alizarin

Fig. 3 Surface roughness (a), water contact angle (b), MTT test (c), ALP activity (d). Note: asterisk, hash, represent $P < 0.05$ when compared with TNTZ group, Ca-P group (or Ca-P-Sr group respectively). Abbreviations: MTT methylthiozol tetrazolium, ALP alkaline phosphatase



Red S and Calcein were observed and indicated the new forming bone (Fig. 9). We analyzed the area of fluorochromes stained bone for Alizarin Red S and Calcein. It turned out that the Ca-P-Sr group displayed a higher Alizarin Red S stained area ($11.30 \pm 1.85\%$) and Calcein stained area ($19.45 \pm 2.61\%$) than Ca-P ($8.63 \pm 1.28\%$, $15.11 \pm 2.41\%$) and TNTZ ($5.00 \pm 1.01\%$, $8.35 \pm 2.34\%$) groups (Fig. 6d).

4 Discussion

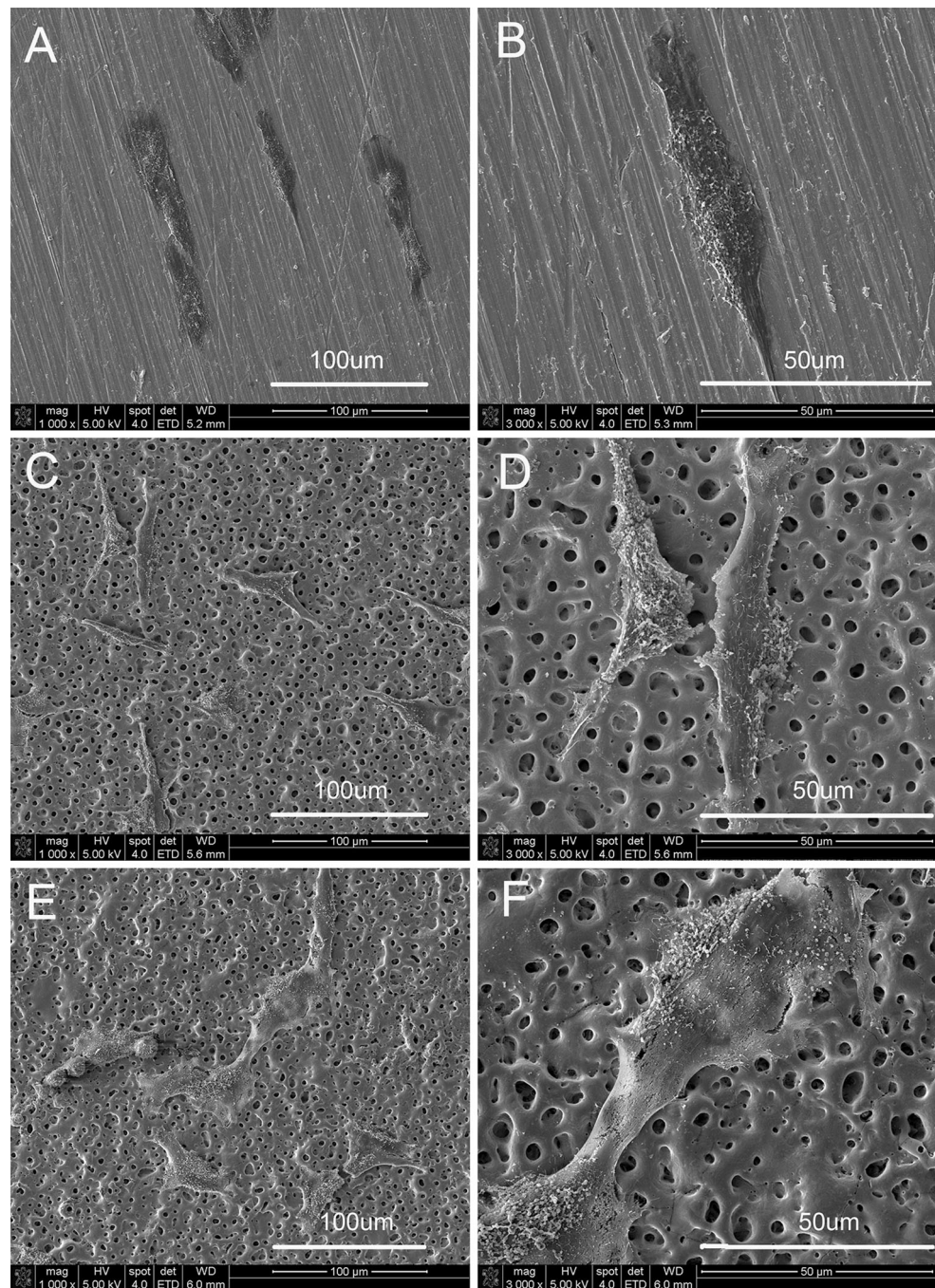
Compared with traditional titanium alloy Ti6Al4V, the novel β -titanium alloy Ti35Nb2Ta3Zr (TNTZ) showed good mechanical characteristics of low Young modulus and contained non-toxic elements [8]. However, the biocompatibility especially the osseointegration ability of TNTZ alloy was unsatisfying. In the present study, we applied MAO to enhance biocompatibility of TNTZ alloy. MAO is a relatively controllable, simple and effective way to modify material's surface. Porous oxide layer coating was formed when went through MAO [29, 30]. We performed MAO process to incorporate Ca, P or Sr into coatings on TNTZ alloys when NaH_2PO_4 , $\text{Ca}(\text{CH}_3\text{COO})_2$, or $\text{Sr}(\text{CH}_3\text{COO})_2$ were added to the electrolyte. Then in vitro and in vivo tests were performed to study the MAOed specimens' biocompatibility and osseointegration ability.

Cell-material interaction has been proved to be associated with chemical and physical properties of materials [31]. Different material properties including roughness, hydrophilicity, surface morphology and chemical composition of material's coating could influence cell-material

interaction [31–33]. In the present study, we determined the characteristics of materials such as surface morphology, roughness, wettability using SEM, AFM and video contact-angle measurement respectively.

Regarding surface morphology, a porous layer was formed when MAO applied to TNTZ alloy, craters existed on the surface of the MAOed specimens (Fig. 1). MAOed groups had a rougher surface than TNTZ alloy (45.52 ± 9.09 nm, 199.44 ± 14.38 nm, 193.38 ± 13.37 nm for TNTZ, Ca-P and Ca-P-Sr groups respectively). However, it was reported that cells would sense a rough surface as smooth if the distance between the surface craters exceed the ability of cells to form focal attachment ($\text{Ra } 3.2\text{--}4.24 \mu\text{m}$) [31, 34]. In our study, the roughness of MAOed alloy is lower than $3 \mu\text{m}$, which indicated that cells can stretch over more than two craters on coating (Fig. 4). Besides, we found more cells on the surface of materials in Ca-P and Ca-P-Sr groups. Actually, We counted cells on the materials per visual field (five fields one sample), which turned out that 21.2 ± 4.3 , 39.6 ± 4.7 , 40.4 ± 5.6 for TNTZ, Ca-P and Ca-P-Sr groups respectively. As Fig. 4a and b showed cells on the TNTZ alloy demonstrated a tighter appearance than MAOed group. Cells on the MAOed group displayed a more pleomorphic shape than TNTZ alloy through the images of SEM, which revealed that cells spread better on MAOed alloy. To be specific, the process of cell adhesion needs the binding of integrins to the extracellular ligands to form pseudopodia [32, 35]. As Fig. 4 showed cells on the surface of the MAOed samples presented a polymorphic shape stretching over the little craters, which inferring that the pseudopodia should attach in the dense craters. While amplifying Fig. 4d and f, some of the pseudopodia were observed stretching into the craters on the surface (Fig. 4).

Fig. 4 SEM results of cells seeded on materials TNTZ group (a, b) Ca-P group (c, d) and Ca-P-Sr group (e, f)



Concerning wettability, some studies argued that it can affect protein adsorption, platelet adhesion/activation, blood coagulation and cell and bacterial adhesion on materials [33, 36]. The adhesion of proteins to a surface is a time-dependent process [31]. An increase in protein adhesion force was observed as the contact angles of the surface decreased below 60° – 65° which was defined as the criterion for “protein adherent” and “protein non-adherent” [37]. In the present study, the contact angles were $39.2^{\circ} \pm 2.9^{\circ}$, $28.7^{\circ} \pm 2.9^{\circ}$, $27.8^{\circ} \pm 3.9^{\circ}$ for TNTZ, Ca-P

and Ca-P-Sr groups respectively, which was considered suitable for cell adhesion [37].

Consistent with cell-counting results by SEM, the MTT revealed the cell viability in MAO coated groups were higher than the TNTZ, which suggested that the MAO coated specimens were more favorable for cell proliferation. As our results demonstrated the MAO coated groups also displayed better ALP activity, which was consensus with some former studies [38, 39] arguing that higher surface roughness and hydrophilicity played an important role on

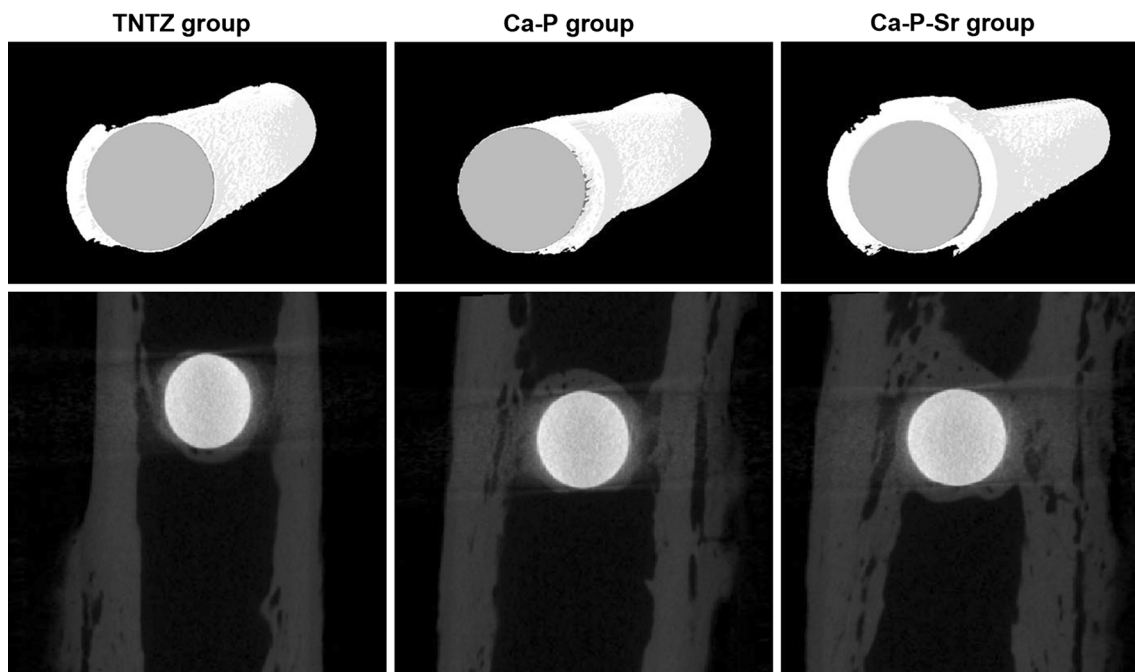
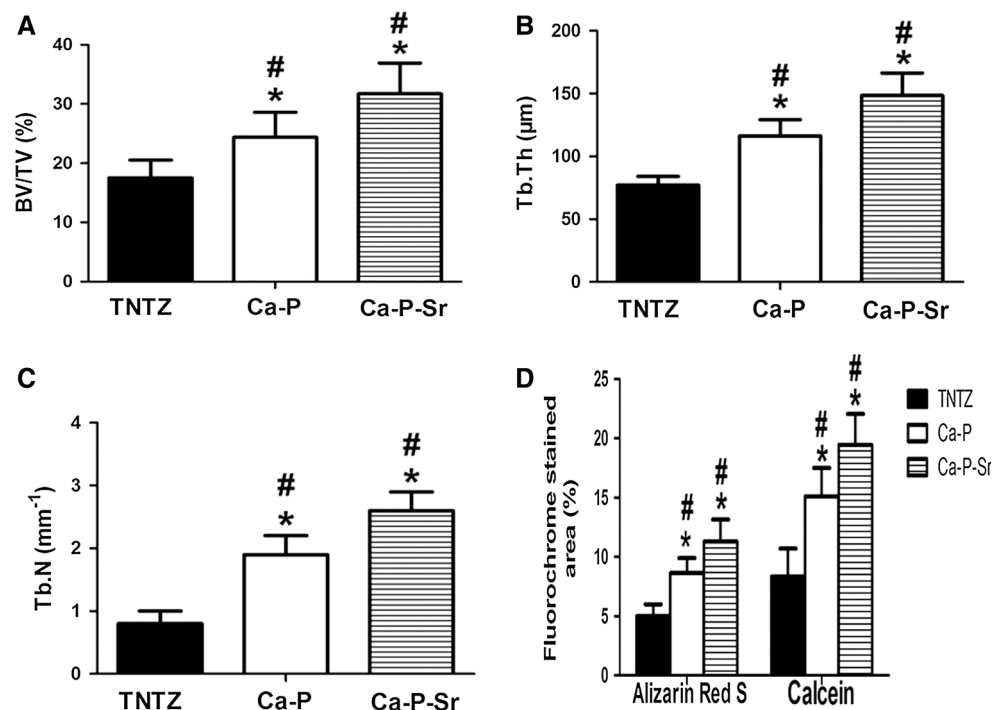


Fig. 5 Micro-CT results of 2D and 3D reconstructed images for the TNTZ group, Ca-P group and Ca-P-Sr group

Fig. 6 The calculated results of micro-CT and sequential fluorescent labeling: BV/TV (a), Tb.Th (b), Th.N (c), area of two fluorochromes stained bone (d). Note: *asterisk, hash*, represent $P < 0.05$ when compared with TNTZ group, Ca-P group (or Ca-P-Sr group respectively). Abbreviations: *BV/TV* bone volume/total volume, *Tb.Th* trabecular thickness, *Th.N* trabecular number

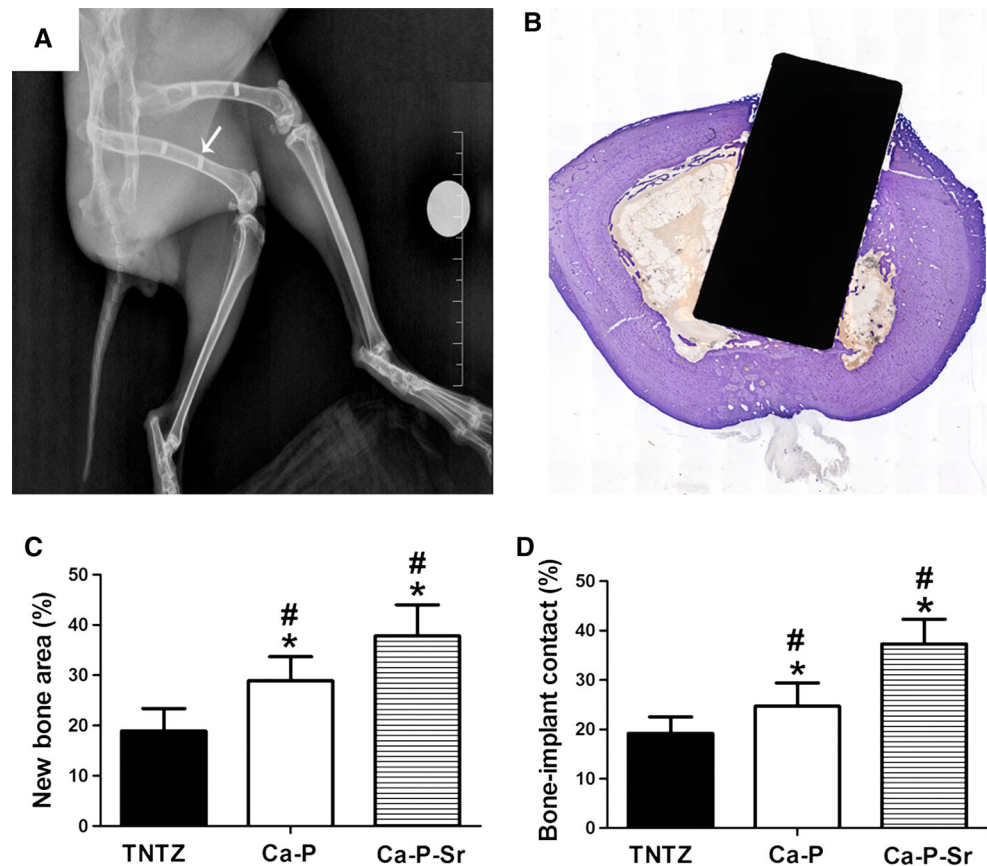


the cells behaviors on materials [40]. However, the cell viability and ALP activity also presented difference between the two MAO coated groups. Despite of the similar surface morphology, the Ca-P-Sr group possessed a better cell viability and ALP activity than the Ca-P group. According to recently studies, we believed that the

strontium added to the coating in Ca-P-Sr group should account for this phenomenon [27, 41].

It was reported that the strontium element affected the osteoblasts and osteoclasts behaviors [22]. As the strontium ranelate was used to treat osteoporosis in some European countries, some studies focused on introducing strontium to

Fig. 7 X-ray image of the rabbit model (*arrow* refers to implant) (**a**), the intersections of implant stained with *toluidine blue* (**b**), results of new bone area (**c**) and bone-implant contact (**d**) in histomorphometric measurements for *toluidine blue* staining. Note: *asterisk, hash*, represent $P < 0.05$ when compared with TNTZ group, Ca-P group (or Ca-P-Sr group respectively) (Color figure online)



the surface of alloys for its potential ability in improving osseointegration [26, 42, 43]. In this study, we performed MAO to incorporate Ca, P or Sr to the layer of TNTZ alloys. The energy dispersive spectroscopy (EDS) conformed that there was 14 wt% Ca and 7 wt% P in Ca-P group, about 8 wt% Sr in Ca-P-Sr group. The difference between the Ca-P group and Ca-P-Sr group in strontium amount may elucidate the enhanced in vitro cells performance and in vivo osseointegration ability. According to some other studies, strontium can activate the CaSR and then trigger the ERK1/2 cascade pathway to promote the osteoblasts proliferation and differentiation [22, 44]. The CaSR was traditionally thought to be a key factor that involved in the calcium homeostasis, predominantly through its effects on the regulation of parathyroid hormone. However, some studies demonstrated that the activation of CaSR can promote the proliferation and differentiation of osteoblasts [45, 46]. Then CaSR senses not only Ca^{2+} but also Sr^{2+} [47]. When the CaSR was activated by Sr^{2+} , the intracellular second messengers DAG and IP_3 were activated then trigger the ERK1/2 cascade pathway [44, 45]. After the phosphorylation of ERK1/2 cascade pathway, more osteoprotegerin (OPG) was synthesized and suppressed the receptor activator of NF- κ B ligand (RANKL) resulting in the promotion of osteoblasts proliferation and differentiation [48, 49].

As to in vivo tests, when experimental rabbits were sacrificed, the micro-CT and histological sections analyses were done to evaluate osseointegration ability of different implants. As we know, the mechanical interlocking force between the bone and implant is a key factor influencing the outcomes of orthopedic or dental surgery. Cell adhesion was the first step of interaction between cells and implant's surface. The more new bone grows and attaches to the implant the more stable it is. In the present study, the micro-CT scanning was performed, by mean of 2D images and 3D reconstruction, finally, all implants were in position, the results demonstrated that more trabecular bone formed around the implant surface in MAOed groups especially Ca-P-Sr group. The histological evaluation was done via light microscopy and confocal laser scanning microscopy. New bone labeled in different fluorochromes was observed. Not only the new forming bone site but also the quantity of new bone was obtained (by means of percentage in stained area). The MAOed groups showed more new bone forming and less gap around the implants. The Ca-P-Sr group displayed a highest osseointegration ability among the three groups. The higher bone forming ability we observed in Ca-P-Sr group than Ca-P group should attribute to the effect of strontium. Previous studies had reported more new bone formation when the local release

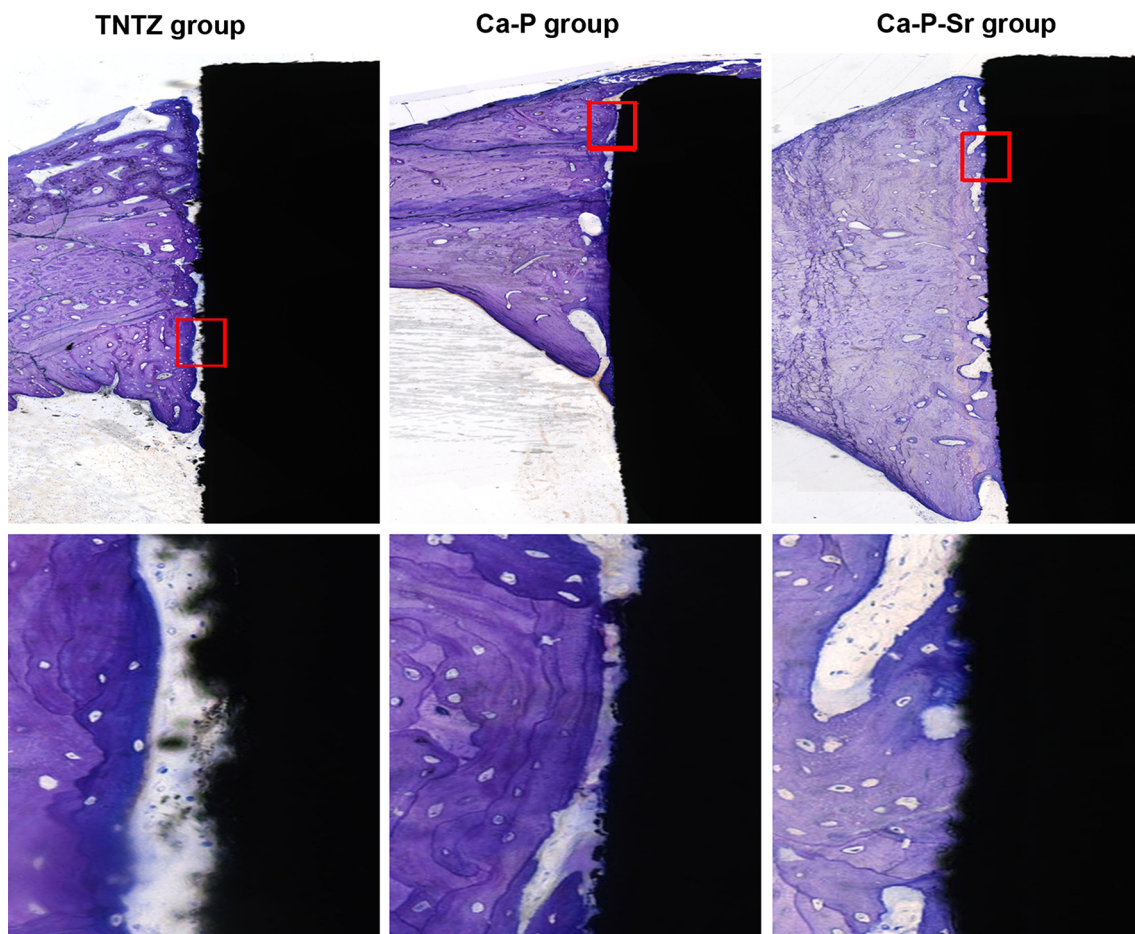


Fig. 8 Toluidine blue staining images of bone-implant area. Red rectangle area was amplified and displayed in the lower panel (Color figure online)

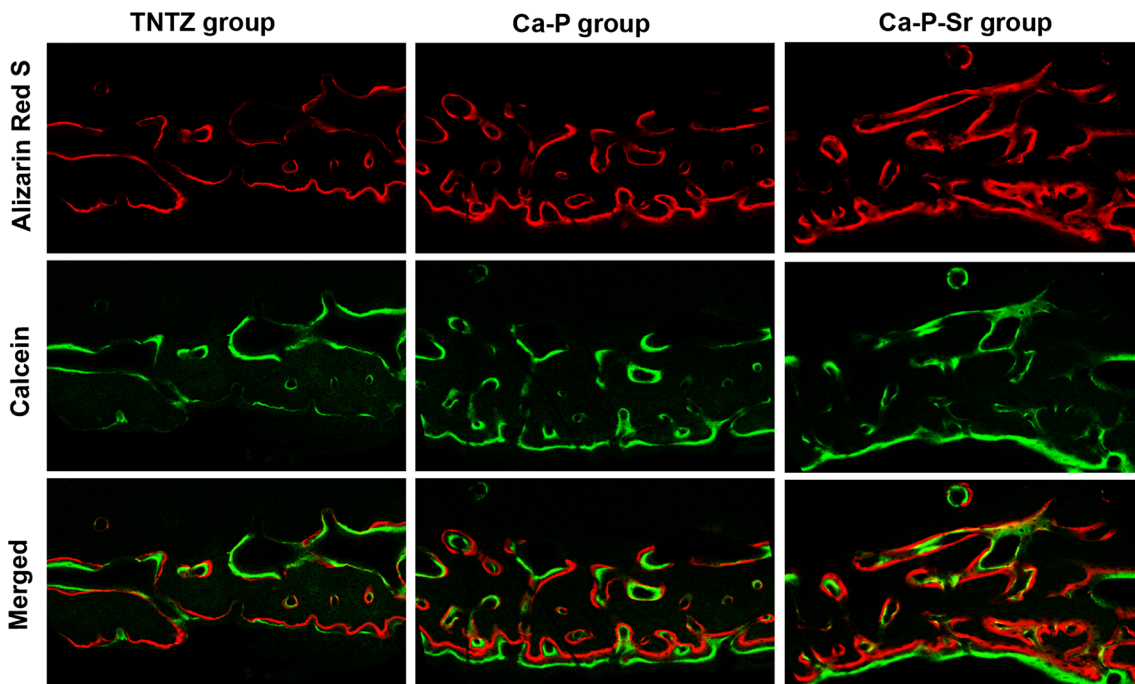


Fig. 9 Sequential fluorescent labeling images of newly forming bone. Alizarin Red S and Calcein were exhibited as red and green respectively (Color figure online)

of Ca, P, Sr [47, 50]. The mechanism of how the strontium affected the bone formation gained its popular recent years. Strontium can promote new bone formation by inhibiting the osteoclasts and boosting osteoblasts through the CaR/ERK1/2 and Wnt signaling pathway [44, 51, 52]. Wnt/b-catenin signaling plays an important role in the bone development and homeostasis [53]. Recently, Fromiguet et al. argued that the Wnt signaling pathway was involved in strontium-induced proliferation and differentiation of the osteoblasts [54]. They demonstrated that the Sr^{2+} activated Wnt/b-catenin signaling, then promoted new bone formation by inhibiting the osteoclasts and boosting osteoblasts through nuclear factor NFATC1 [54, 55]. Some studies also reported that different levels of Sr^{2+} concentration may lead to different results of new bone formation and side effects, which meaning that the accumulation of Sr^{2+} should be paid attention to when applied to human [56, 57]. The future study about the biocompatibility of different contents of Sr^{2+} in MAO coated TNTZ alloy would be performed soon.

5 Conclusions

The Ca–P and Ca–P–Sr TNTZ alloys were successfully synthesized through MAO process. In vitro tests demonstrated that the MAOed groups displayed better cells' adhesion, proliferation, differentiation ability than TNTZ alloy. More new bone formation was observed in the MAOed groups than in TNTZ group through the in vivo experiment. The Ca–P–Sr TNTZ showed a better osseointegration than Ca–P TNTZ alloy. The Ca–P–Sr TNTZ may be a promising biomedical material for orthopedic or dental use. The best suitable content of strontium in Ca–P–Sr TNTZ would be further investigated.

Acknowledgments The present study was supported by the National Natural Science Foundation of China (Grant Nos. 81271962 and 81171688), The Science and Technology Commission of Shanghai Municipality, China (Grant No. 12jc1407302).

Compliance with Ethical Standards

Conflict of interest The authors declared no conflicts of interest in this work.

References

- Hao YL, Li SJ, Sun BB, Sui ML, Yang R. Ductile titanium alloy with low Poisson's ratio. *Phys Rev Lett*. 2007;98(21):216405.
- Wang K. The use of titanium for medical applications in the USA. *Mater Sci Eng A*. 1996;213(1):134–7.
- Snyder SM, Schneider E. Estimation of mechanical properties of cortical bone by computed tomography. *J Orthop Res*. 1991;9(3):422–31. doi:10.1002/jor.1100090315.
- Gefen A. Computational simulations of stress shielding and bone resorption around existing and computer-designed orthopaedic screws. *Med Biol Eng Comput*. 2002;40(3):311–22.
- Rehder D. Vanadium. its role for humans. *Metal ions in life sciences*. 2013;13:139–69. doi:10.1007/978-94-007-7500-8_5.
- Goyer RA, Clarkson TW. Toxic effects of metals. In: Klaassen CD, editors. *Casarett & Doull's toxicology the basic science of poisons*, 5th ed. New York: McGraw-Hill Health Professions Division; 1996. ISBN 71054766.
- Long M, Rack HJ. Titanium alloys in total joint replacement—a materials science perspective. *Biomaterials*. 1998;19(18):1621–39.
- Guo Y, Chen D, Lu W, Jia Y, Wang L, Zhang X. Corrosion resistance and in vitro response of a novel Ti35Nb2Ta3Zr alloy with a low Young's modulus. *Biomed Mater*. 2013;8(5):055004. doi:10.1088/1748-6041/8/5/055004.
- Guo Y, Chen D, Cheng M, Lu W, Wang L, Zhang X. The bone tissue compatibility of a new Ti35Nb2Ta3Zr alloy with a low Young's modulus. *Int J Mol Med*. 2013;31(3):689–97. doi:10.3892/ijmm.2013.1249.
- Hu H, Qiao Y, Meng F, Liu X, Ding C. Enhanced apatite-forming ability and cytocompatibility of porous and nanostructured TiO₂/CaSiO₃ coating on titanium. *Colloids Surf B*. 2013;101:83–90. doi:10.1016/j.colsurfb.2012.06.021.
- Wang G, Lu Z, Liu X, Zhou X, Ding C, Zreiqat H. Nanostructured glass-ceramic coatings for orthopaedic applications. *J R Soc Interface*. 2011;8(61):1192–203. doi:10.1098/rsif.2010.0680.
- Chen XB, Li YC, Du Plessis J, Hodgson PD, Wen C. Influence of calcium ion deposition on apatite-inducing ability of porous titanium for biomedical applications. *Acta Biomater*. 2009;5(5):1808–20. doi:10.1016/j.actbio.2009.01.015.
- Treves C, Martinesi M, Stio M, Gutierrez A, Jimenez JA, Lopez MF. In vitro biocompatibility evaluation of surface-modified titanium alloys. *J Biomed Mater Res A*. 2010;92(4):1623–34. doi:10.1002/jbm.a.32507.
- Heimann RB, Wirth R. Formation and transformation of amorphous calcium phosphates on titanium alloy surfaces during atmospheric plasma spraying and their subsequent in vitro performance. *Biomaterials*. 2006;27(6):823–31. doi:10.1016/j.biomaterials.2005.06.029.
- Xie Y, Liu X, Huang A, Ding C, Chu PK. Improvement of surface bioactivity on titanium by water and hydrogen plasma immersion ion implantation. *Biomaterials*. 2005;26(31):6129–35. doi:10.1016/j.biomaterials.2005.03.032.
- Wei D, Zhou Y, Jia D, Wang Y. Characteristic and in vitro bioactivity of a microarc-oxidized TiO₂-based coating after chemical treatment. *Acta Biomater*. 2007;3(5):817–27. doi:10.1016/j.actbio.2007.03.001.
- Boanini E, Gazzano M, Bigi A. Ionic substitutions in calcium phosphates synthesized at low temperature. *Acta Biomater*. 2010;6(6):1882–94. doi:10.1016/j.actbio.2009.12.041.
- Bracci B, Torricelli P, Panzavolta S, Boanini E, Giardino R, Bigi A. Effect of Mg²⁺, Sr²⁺, and Mn²⁺ on the chemico-physical and in vitro biological properties of calcium phosphate biomimetic coatings. *J Inorg Biochem*. 2009;103(12):1666–74. doi:10.1016/j.jinorgbio.2009.09.009.
- Kuo MC, Yen SK. The process of electrochemical deposited hydroxyapatite coatings on biomedical titanium at room temperature. *Mater Sci Eng C*. 2002;20(1–2):153–60. doi:10.1016/S0928-4931(02)00026-7.
- Dahl SG, Allain P, Marie PJ, Mauras Y, Boivin G, Ammann P, Tsouderos Y, Delmas PD, Christiansen C. Incorporation and distribution of strontium in bone. *Bone*. 2001;28(4):446–53. doi:10.1016/S8756-3282(01)00419-7.
- Meunier PJ, Roux C, Ortolani S, Diaz-Curiel M, Compston J, Marquis P, Cormier C, Isaia G, Badurski J, Wark JD, Collette J, Reginster JY. Effects of long-term strontium ranelate treatment

- on vertebral fracture risk in postmenopausal women with osteoporosis. *Osteoporos Int*. 2009;20(10):1663–73. doi:[10.1007/s00198-008-0825-6](https://doi.org/10.1007/s00198-008-0825-6).
22. Bonnelye E, Chabadel A, Saltel F, Jurdic P. Dual effect of strontium ranelate: stimulation of osteoblast differentiation and inhibition of osteoclast formation and resorption in vitro. *Bone*. 2008;42(1):129–38. doi:[10.1016/j.bone.2007.08.043](https://doi.org/10.1016/j.bone.2007.08.043).
 23. Peng S, Liu XS, Huang S, Li Z, Pan H, Zhen W, Luk KD, Guo XE, Lu WW. The cross-talk between osteoclasts and osteoblasts in response to strontium treatment: involvement of osteoprotegerin. *Bone*. 2011;49(6):1290–8. doi:[10.1016/j.bone.2011.08.031](https://doi.org/10.1016/j.bone.2011.08.031).
 24. Zhao L, Wang H, Huo K, Zhang X, Wang W, Zhang Y, Wu Z, Chu PK. The osteogenic activity of strontium loaded titania nanotube arrays on titanium substrates. *Biomaterials*. 2013;34(1):19–29. doi:[10.1016/j.biomaterials.2012.09.041](https://doi.org/10.1016/j.biomaterials.2012.09.041).
 25. Fu DL, Jiang QH, He FM, Yang GL, Liu L. Fluorescence microscopic analysis of bone osseointegration of strontium-substituted hydroxyapatite implants. *J Zhejiang Univ Sci B*. 2012;13(5):364–71. doi:[10.1631/jzus.B1100381](https://doi.org/10.1631/jzus.B1100381).
 26. Li Y, Li Q, Zhu S, Luo E, Li J, Feng G, Liao Y, Hu J. The effect of strontium-substituted hydroxyapatite coating on implant fixation in ovariectomized rats. *Biomaterials*. 2010;31(34):9006–14. doi:[10.1016/j.biomaterials.2010.07.112](https://doi.org/10.1016/j.biomaterials.2010.07.112).
 27. Matsunaga K, Murata H. Strontium substitution in bioactive calcium phosphates: a first-principles study. *J Phys Chem B*. 2009;113(11):3584–9. doi:[10.1021/jp808713m](https://doi.org/10.1021/jp808713m).
 28. Zhang W, Wang G, Liu Y, Zhao X, Zou D, Zhu C, Jin Y, Huang Q, Sun J, Liu X, Jiang X, Zreiqat H. The synergistic effect of hierarchical micro/nano-topography and bioactive ions for enhanced osseointegration. *Biomaterials*. 2013;34(13):3184–95. doi:[10.1016/j.biomaterials.2013.01.008](https://doi.org/10.1016/j.biomaterials.2013.01.008).
 29. dos Santos A, Araujo JR, Landi SM, Kuznetsov A, Granjeiro JM, de Sena LA, Achete CA. A study of the physical, chemical and biological properties of TiO₂ coatings produced by micro-arc oxidation in a Ca–P-based electrolyte. *J Mater Sci Mater Med*. 2014;25(7):1769–80. doi:[10.1007/s10856-014-5207-3](https://doi.org/10.1007/s10856-014-5207-3).
 30. Li LH, Kong YM, Kim HW, Kim YW, Kim HE, Heo SJ, Koak JY. Improved biological performance of Ti implants due to surface modification by micro-arc oxidation. *Biomaterials*. 2004;25(14):2867–75. doi:[10.1016/j.biomaterials.2003.09.048](https://doi.org/10.1016/j.biomaterials.2003.09.048).
 31. Ventre M, Causa F, Netti PA. Determinants of cell-material crosstalk at the interface: towards engineering of cell instructive materials. *J R Soc Interface*. 2012;9(74):2017–32. doi:[10.1098/rsif.2012.0308](https://doi.org/10.1098/rsif.2012.0308).
 32. Parsons JT, Horwitz AR, Schwartz MA. Cell adhesion: integrating cytoskeletal dynamics and cellular tension. *Nat Rev Mol Cell Biol*. 2010;11(9):633–43. doi:[10.1038/nrm2957](https://doi.org/10.1038/nrm2957).
 33. Vogler EA. Water and the acute biological response to surfaces. *J Biomater Sci Polym Ed*. 1999;10(10):1015–45.
 34. Lincks J, Boyan BD, Blanchard CR, Lohmann CH, Liu Y, Cochran DL, Dean DD, Schwartz Z. Response of MG63 osteoblast-like cells to titanium and titanium alloy is dependent on surface roughness and composition. *Biomaterials*. 1998;19(23):2219–32.
 35. del Rio A, Perez-Jimenez R, Liu R, Roca-Cusachs P, Fernandez JM, Sheetz MP. Stretching single talin rod molecules activates vinculin binding. *Science*. 2009;323(5914):638–41. doi:[10.1126/science.1162912](https://doi.org/10.1126/science.1162912).
 36. Sethuraman A, Han M, Kane RS, Belfort G. Effect of surface wettability on the adhesion of proteins. *Langmuir*. 2004;20(18):7779–88. doi:[10.1021/la049454q](https://doi.org/10.1021/la049454q).
 37. Xu LC, Siedlecki CA. Effects of surface wettability and contact time on protein adhesion to biomaterial surfaces. *Biomaterials*. 2007;28(22):3273–83. doi:[10.1016/j.biomaterials.2007.03.032](https://doi.org/10.1016/j.biomaterials.2007.03.032).
 38. Rausch-fan X, Qu Z, Wieland M, Matejka M, Schedle A. Differentiation and cytokine synthesis of human alveolar osteoblasts compared to osteoblast-like cells (MG63) in response to titanium surfaces. *Dent Mater*. 2008;24(1):102–10. doi:[10.1016/j.dental.2007.03.001](https://doi.org/10.1016/j.dental.2007.03.001).
 39. Qu Z, Rausch-Fan X, Wieland M, Matejka M, Schedle A. The initial attachment and subsequent behavior regulation of osteoblasts by dental implant surface modification. *J Biomed Mater Res A*. 2007;82(3):658–68. doi:[10.1002/jbm.a.31023](https://doi.org/10.1002/jbm.a.31023).
 40. Wennerberg A, Albrektsson T. On implant surfaces: a review of current knowledge and opinions. *Int J Oral Maxillofac Implant*. 2010;25(1):63–74.
 41. Oliveira AL, Reis RL, Li P. Strontium-substituted apatite coating grown on Ti6Al4V substrate through biomimetic synthesis. *J Biomed Mater Res B Appl Biomater*. 2007;83(1):258–65. doi:[10.1002/jbm.b.30791](https://doi.org/10.1002/jbm.b.30791).
 42. Li Y, Li X, Song G, Chen K, Yin G, Hu J. Effects of strontium ranelate on osseointegration of titanium implant in osteoporotic rats. *Clin Oral Implant Res*. 2012;23(9):1038–44. doi:[10.1111/j.1600-0501.2011.02252.x](https://doi.org/10.1111/j.1600-0501.2011.02252.x).
 43. Maimoun L, Brennan TC, Badoud I, Dubois-Ferriere V, Rizzoli R, Ammann P. Strontium ranelate improves implant osseointegration. *Bone*. 2010;46(5):1436–41. doi:[10.1016/j.bone.2010.01.379](https://doi.org/10.1016/j.bone.2010.01.379).
 44. Chattopadhyay N, Quinn SJ, Kifor O, Ye C, Brown EM. The calcium-sensing receptor (CaR) is involved in strontium ranelate-induced osteoblast proliferation. *Biochem Pharmacol*. 2007;74(3):438–47. doi:[10.1016/j.bcp.2007.04.020](https://doi.org/10.1016/j.bcp.2007.04.020).
 45. Yamaguchi T. The calcium-sensing receptor in bone. *J Bone Miner Metab*. 2008;26(4):301–11. doi:[10.1007/s00774-008-0843-7](https://doi.org/10.1007/s00774-008-0843-7).
 46. Dvorak MM, Siddiqua A, Ward DT, Carter DH, Dallas SL, Nemeth EF, Riccardi D. Physiological changes in extracellular calcium concentration directly control osteoblast function in the absence of calciotropic hormones. *Proc Natl Acad Sci USA*. 2004;101(14):5140–5. doi:[10.1073/pnas.0306141101](https://doi.org/10.1073/pnas.0306141101).
 47. Coulombe J, Faure H, Robin B, Ruat M. In vitro effects of strontium ranelate on the extracellular calcium-sensing receptor. *Biochem Biophys Res Commun*. 2004;323(4):1184–90. doi:[10.1016/j.bbrc.2004.08.209](https://doi.org/10.1016/j.bbrc.2004.08.209).
 48. Brennan TC, Rybchyn MS, Green W, Atwa S, Conigrave AD, Mason RS. Osteoblasts play key roles in the mechanisms of action of strontium ranelate. *Br J Pharmacol*. 2009;157(7):1291–300. doi:[10.1111/j.1476-5381.2009.00305.x](https://doi.org/10.1111/j.1476-5381.2009.00305.x).
 49. Walsh MC, Kim N, Kadono Y, Rho J, Lee SY, Lorenzo J, Choi Y. Osteoimmunology: interplay between the immune system and bone metabolism. *Annu Rev Immunol*. 2006;24(1):33–63. doi:[10.1146/annurev.immunol.24.021605.090646](https://doi.org/10.1146/annurev.immunol.24.021605.090646).
 50. Offermanns V, Andersen OZ, Falkensammer G, Andersen IH, Almtoft KP, Sorensen S, Sillassen M, Jeppesen CS, Rasse M, Foss M, Kloss F. Enhanced osseointegration of endosseous implants by predictable sustained release properties of strontium. *J Biomed Mater Res B Appl Biomater*. 2014;. doi:[10.1002/jbm.b.33279](https://doi.org/10.1002/jbm.b.33279).
 51. Yamaguchi S, Nath S, Matsushita T, Kokubo T. Controlled release of strontium ions from a bioactive Ti metal with a Ca-enriched surface layer. *Acta Biomater*. 2014;10(5):2282–9. doi:[10.1016/j.actbio.2014.01.026](https://doi.org/10.1016/j.actbio.2014.01.026).
 52. Saidak Z, Hay E, Marty C, Barbara A, Marie PJ. Strontium ranelate rebalances bone marrow adipogenesis and osteoblastogenesis in senescent osteopenic mice through NFATc/Maf and Wnt signaling. *Aging Cell*. 2012;11(3):467–74. doi:[10.1111/j.1474-9726.2012.00804.x](https://doi.org/10.1111/j.1474-9726.2012.00804.x).
 53. Minear S, Leucht P, Jiang J, Liu B, Zeng A, Fuerer C, Nusse R, Helms JA. Wnt proteins promote bone regeneration. *Sci Transl Med*. 2010;2(29):29ra30. doi:[10.1126/scitranslmed.3000231](https://doi.org/10.1126/scitranslmed.3000231).
 54. Fromigou O, Hay E, Barbara A, Marie PJ. Essential role of nuclear factor of activated T cells (NFAT)-mediated Wnt signaling in osteoblast differentiation induced by strontium ranelate. *J Biol Chem*. 2010;285(33):25251–8. doi:[10.1074/jbc.M110.110502](https://doi.org/10.1074/jbc.M110.110502).
 55. Almeida M, Han L, Martin-Millan M, O'Brien CA, Manolagas SC. Oxidative stress antagonizes Wnt signaling in osteoblast

- precursors by diverting beta-catenin from T cell factor- to fork-head box O-mediated transcription. *J Biol Chem.* 2007;282(37):27298–305. doi:[10.1074/jbc.M702811200](https://doi.org/10.1074/jbc.M702811200).
56. Yan J, Sun JF, Chu PK, Han Y, Zhang YM. Bone integration capability of a series of strontium-containing hydroxyapatite coatings formed by micro-arc oxidation. *J Biomed Mater Res A.* 2013;101(9):2465–80. doi:[10.1002/jbm.a.34548](https://doi.org/10.1002/jbm.a.34548).
57. Schrooten I, Behets GJ, Cabrera WE, Vercauteren SR, Lamberts LV, Verberckmoes SC, Bervoets AJ, Dams G, Goodman WG, De Broe ME, D'Haese PC. Dose-dependent effects of strontium on bone of chronic renal failure rats. *Kidney Int.* 2003;63(3):927–35. doi:[10.1046/j.1523-1755.2003.00809.x](https://doi.org/10.1046/j.1523-1755.2003.00809.x).